


Article

Environmental Risk Source Analysis and Classification of Zones: Subway Construction

Yangchun Yuan ^{1,2}, Yongjun Qin ^{1,2,*} , Yongkang Zhang ³, Liangfu Xie ^{1,2}, Xin Meng ¹ and Zheyi Guo ¹

¹ School of Civil Engineering and Architecture, Xinjiang University, Urumqi 830047, China; yangchun1668@163.com (Y.Y.); xieliangfu@xju.edu.cn (L.X.); mengxin@stu.xju.edu.cn (X.M.); 875715741@stu.xju.edu.cn (Z.G.)

² Xinjiang Civil Engineering Technology Research Center, Urumqi 830016, China

³ CCFEB Civil Engineering Co., Ltd., Changsha 410004, China; zhangyongkangzjwj@163.com

* Correspondence: qyjg@xju.edu.cn

Abstract: Examining the environmental risk sources of regional subway construction is crucial for ensuring construction safety and providing guidance for future subway line planning. This study focused on Urumqi's main urban area and used SBAS-InSAR analysis technology to extract the settlement rate field within 600 m of Urumqi Metro Line 1 and investigate these risk sources. Results showed that the environmental risk sources affecting subway construction in the study area could be classified into four categories: geological conditions, distribution of high-rise buildings, density of road networks, and density of clustered buildings. The study further analyzed the spatial distribution of each risk source and developed a comprehensive impact zoning evaluation model for environmental risk sources in the study area. The model was then used to assess the risk of the currently planned subway lines (1–7), revealing that the largest area of subway construction environmental risk sources (1444 partitions) was associated with soil layer, IV high-rise building risk, IV road network risk, and IV building density risk. Additionally, the study found that environmental risk sources had the most significant impact on Metro Line 6, emphasizing the importance of closely monitoring risk factors during future construction.

Keywords: subway construction; risk source; distribution characteristics; comprehensive impact zoning



Citation: Yuan, Y.; Qin, Y.; Zhang, Y.; Xie, L.; Meng, X.; Guo, Z.

Environmental Risk Source Analysis and Classification of Zones: Subway Construction. *Appl. Sci.* **2023**, *13*, 5831. <https://doi.org/10.3390/app13105831>

Academic Editor: Francesco Colangelo

Received: 9 March 2023

Revised: 7 April 2023

Accepted: 10 April 2023

Published: 9 May 2023



Copyright: © 2023 by the authors. Licensee MDPI, Basel, Switzerland. This article is an open access article distributed under the terms and conditions of the Creative Commons Attribution (CC BY) license (<https://creativecommons.org/licenses/by/4.0/>).

1. Introduction

The subway plays a crucial role in guiding and coordinating urban development and construction in China, and it has gradually become a vital component of the country's urban traffic development. However, the risk of subway construction is closely related to urban development due to the characteristics of subway use. The complex and constantly changing construction environment of the city and certain human activities have resulted in various types of environmental risk sources for subway construction, which can cause different levels of settlement during construction [1,2]. This can significantly impact the safety of people's lives and property.

The extended duration of subway construction exposes it to various risks, underscoring the need to assess these risks comprehensively. Researchers worldwide have pursued various analytical approaches to assess subway construction risk. For instance, Zhang et al. [3] adopted an analytical hierarchy process (AHP) model that incorporated factors such as rock mass comprehensive degree, lithology characteristics, geological structure characteristics, weathering degree, seismic intensity, slope, rainfall, and construction factors to identify and rank tunnel portal slope stability. Yu et al. [4] proposed a probabilistic risk analysis technique that uses a layered simulation model to analyze risk factors at the tunnel construction operation level. Similarly, Zhou et al. [5] advocated for analyzing subway construction safety risks by establishing a database of accidents encountered during the construction process. Liu et al. [6] proposed a novel risk assessment technique that

combines AHP and an expert classification method (EGM) to evaluate how geological conditions and the surrounding environment affect subway construction. Finally, Fu et al. [7] used the Apriori algorithm to mine robust association rules between risks in subway deep foundation pit engineering. Their findings suggest that key risk groups emanate from factors related to contractors, structures, and the natural environment, whereas the core sources of risk are attributable to owners, designers, and the social environment. However, these studies reveal that the construction environment exerts a significant influence on subway construction risk, but the analytical techniques employed incorporate subjective factors that do not reflect the environmental impact objectively.

The subway construction environment and risk are interrelated, and several scholars worldwide have studied the risks that arise from the subway construction environment [8–11]. For example, Xiao [12] conducted numerical simulation analysis to summarize how high-rise buildings affect subway stations and station ancillary facilities. The study established that the excavation of tunnels disrupts the original stress balance state, making the new tunnel structure vulnerable to the large load of super high-rise buildings. Shen [13] employed finite element analysis software to study the impact of super high-rise building structures on adjacent subway tunnels. The research found that during the structural construction stage, the tunnel mainly experiences vertical settlement, with minimal horizontal displacement. However, during the use stage of super high-rise buildings, the tunnel's settlement and horizontal deformation change. XUE et al. [14] investigated how geological and hydrological conditions impact tunnels, and they established that groundwater conditions and rock integrity are the main factors leading to soft rock tunnel collapse. Xu et al. [15] used surrounding rock lithology, topography, excavation span, buried depth, groundwater, and rainfall as rating indicators to evaluate the collapse risk of loess tunnels. Meng et al. [16] proposed a cloud model and fuzzy analytic hierarchy process-based risk assessment method that established a risk assessment index system comprising four first-level indicators and seventeen second-level indicators, such as karst geological conditions, hydrogeological conditions, tunnel design, and shield construction. Adverse geological conditions were found to have the most significant impact on shield construction risk. Zhou et al. [17] studied the risk of urban subway tunnels crossing existing bridge pile foundations, and they identified pile foundation settlement as the primary risk. Li et al. [18] investigated the response of subway tunnels to dynamic vehicle loads and found that subway shield tunnel displacement amplitude and soil maximum settlement were significantly affected by vehicle load. Shi et al. [19] analyzed the displacement changes of underground tunnels and building foundation pit excavation, and they established that the connection area between the tunnel and the foundation pit experiences minimal horizontal displacement, while the tunnel experiences significant vertical displacement, and settlement at the corner of the building adjacent to the foundation pit is relatively high. Xu et al. [20] analyzed subway construction settlement when crossing existing railways and identified train live load as the main factor leading to subway construction settlement. While these studies highlight risk sources associated with individual subways in different regions of China, the actual subway construction environment typically faces multiple risk sources, necessitating the development of a method that considers the comprehensive impact of risk sources in the study area and accurately evaluates each risk source's risk level.

Based on the preceding analysis and discussion, it is apparent that the distribution of environmental risk sources in subway construction varies regionally. Therefore, identifying risk sources based on regional characteristics can enhance the accuracy of results. Risk identification involves investigating and recognizing potential risks in the subway construction process and categorizing them based on risk types and impact levels. An analysis of various types of subway construction accidents reveals that most accidents occur due to surface subsidence caused by the subway construction process [21,22]. Regional surface subsidence can be regarded as an indication of the distribution of environmental risk sources to a certain degree [23–27].

The research area for this study is Urumqi, which is situated at the center of Eurasia, at the northern foot of the Tianshan Mountains, and at the southern edge of the Junggar Basin. As the capital of the Xinjiang Uygur Autonomous Region, Urumqi is the political, economic, and cultural hub of the region and serves as the western bridgehead of China, playing a significant role in China's Belt and Road Initiative. With the development of Urumqi as the core economic zone, the demand for rail transit has been on the rise. According to the "Urumqi Rail Transit Network Planning", the planned length of Urumqi's rail transit line is 261.8 kilometers, with Line 1~7 being the main city planning line. In 2019, Urumqi Metro Line 1 was completed and put into operation, while Line 2 began construction in 2015, and the first phase of Metro Line 3 and Line 4 began construction in 2016.

Conventional methods for monitoring subway settlement do not provide a comprehensive overview. Interferometric Synthetic Aperture Radar (InSAR) is a satellite-based technology that offers several advantages, including high resolution, high precision, wide range, and all-weather, all-day monitoring [28–31]. It has proven successful in monitoring surface deformation in various regions. This study employs the SBAS-InSAR [32–34] analysis method to derive the surface deformation rate field during the construction of Urumqi's existing subway line 1. Examining surface deformation in the area along subway line 1 during construction can identify the environmental factors responsible for such deformation and uncover potential risk sources associated with subway construction [35–38]. By calibrating these environmental risk sources, we analyze the geometric distribution of each risk source using ArcGIS software. We then overlay the distribution characteristics of each risk source to assess and partition the environmental risks associated with subway construction. This study offers insight into future Urumqi subway line planning and subway construction risk assessment.

2. Urumqi Engineering Geological Survey

Urumqi is situated in the heartland of Eurasia, at the northern foot of the Northern Tianshan Mountains and the southern edge of the Junggar Basin. The city is surrounded by mountains on its east, south, and west sides. The terrain is high in the southeast and low in the northwest, located at $86^{\circ}37'33''$ – $88^{\circ}58'24''$ E and $42^{\circ}45'32''$ – $44^{\circ}08'00''$ N, with an altitude ranging from 580–920 m and a natural slope of 12%–15%. The city comprises seven districts and one county (Tianshan District, Shayibake District, Xinshi District, Shuimogou District, Toutunhe District, Dabancheng District, Midong District, and Urumqi County) and covers a total area of 14,216 km², of which 2813 km² is the built-up area.

Subway construction predominantly occurs in urban centers. To gain an understanding of the study area's city planning and subway line development, we obtained Urumqi's 2020 land-use data from ESA (Figure 1a) and Urumqi's rail transit planning data (Figure 1b) from the Urumqi Metro Group. Figure 1a was generated by Esri, Impact Observatory, and Microsoft based on Sentinel-2 10 m resolution satellite data. Figure 1b represents the "Urumqi Rail Transit Construction Plan 2012–2019", which the China National Development and Reform Commission approved in 2005. As of 2023, the construction and utilization of Urumqi Metro Line 1 and the first phase of Urumqi Metro Line 2, 3, and 4 have been completed.

To identify the research area, we drew the contour grid map of the primary urban region using the cadastral processing function of Arc GIS, combined with Urumqi's land-use planning map. We excluded scattered building areas and confined the study area to Urumqi's northwest, covering 2813 km².

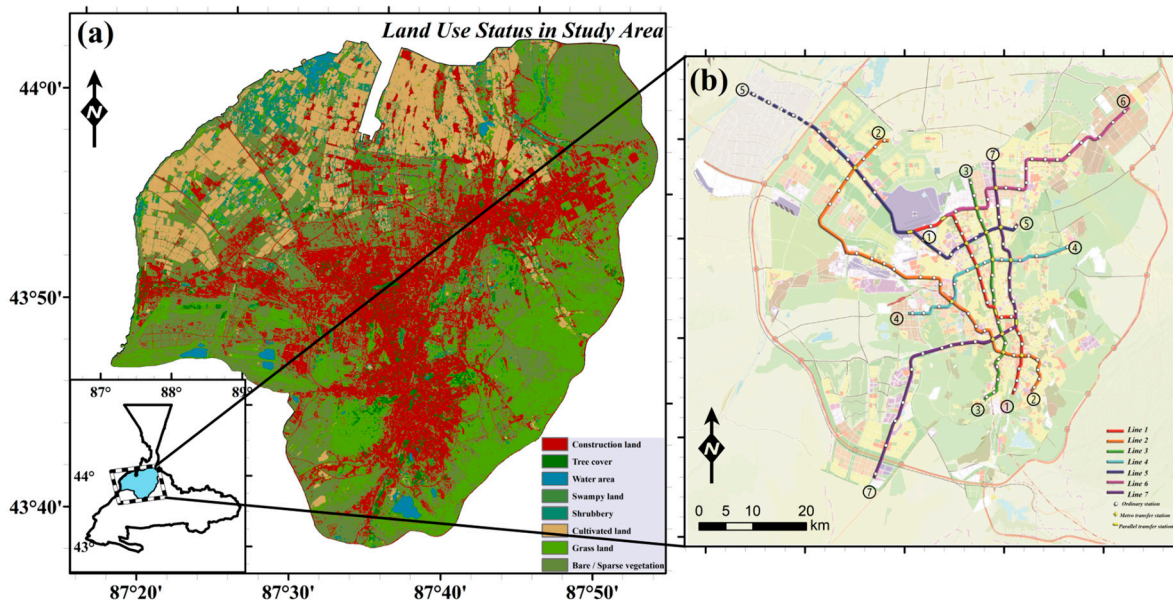


Figure 1. Study area coverage and land use data map. (a) Distribution of land use data in the study area in 2021; (b) planning map of Urumqi subway line, including Lines 1, 2, 3, 4, 5, 6, and 7.

3. Risk Source Analysis of Subway Construction

3.1. Introduction of SBAS-InSAR

Small Base Line Subset Interferometric Synthetic Aperture Radar (SBAS-InSAR) is a satellite-based monitoring technique that offers all-weather, all-day, high-resolution, high-precision, wide-range, and convenient data acquisition advantages. This technology can accurately measure surface deformation at a millimeter level, with high spatial resolution and wide coverage. Given its unique benefits, it has considerable potential in monitoring land subsidence over large areas and long-time periods and has been successfully applied in various regions for surface deformation monitoring.

Compared to traditional geodetic methods, such as leveling and topographic surveys, SBAS-InSAR technology overcomes limitations such as manual distribution, low spatial resolution, and high cost. SBAS-InSAR technology can provide a comprehensive view of the subsidence process along the subway and subsequently identify changes in ground deformation in time and space. The flow chart of SBAS-InSAR is presented in Figure 2.

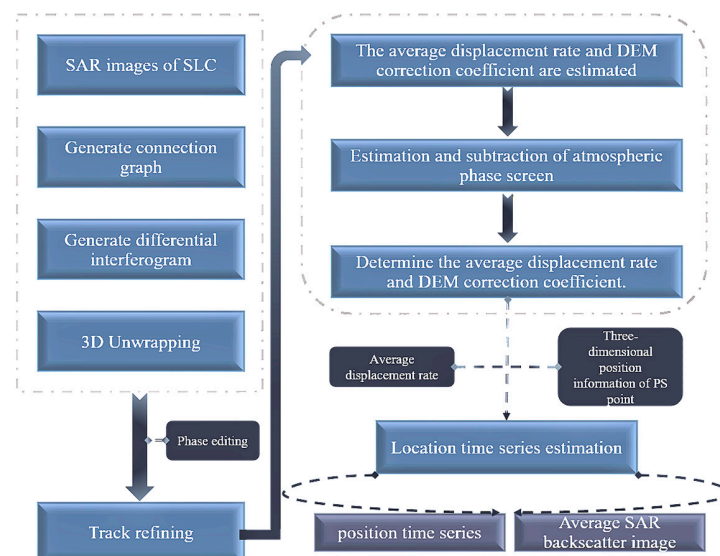


Figure 2. SBAS-InSAR workflow flow chart.

Urumqi Metro Line 1 starts at Santunbei Station in Tianshan District and passes through Tianshan District, Shayibake District, Shuimogou District, and Xinshi District, with stops at Santunbei, Xinjiang University, International Bazaar, Nanhu Square (People's Government of Urumqi City), and the international airport station line in Xinshi District. The line covers a distance of 27.615 km and commenced operation on 28 June 2019. It is an underground line with 21 stations and runs roughly in a north–south direction.

The study area focuses on surface deformation during the subway construction. This study used surface deformation driving factors during the construction of Urumqi Metro Line 1 to determine and identify environmental risk sources during subway construction. The study obtained 22 satellite images from Sentinel-1A between 2017 and 2018 to extract the deformation rate field along the 600 m range of Metro Line 1 using SBAS-InSAR technology [39]. By studying the regional differences in deformation rate during the construction of Urumqi Metro Line 1 and combining this data with the characteristic environmental risk sources of each region, the study compared the surface deformation performance of different construction areas to determine environmental risk sources of subway construction in the study area [40].

3.2. Geological Conditions

Surface subsidence associated with subway construction is closely related to regional geological conditions, affecting the construction methods used for the subway sections. Different construction methods result in varying degrees of surface subsidence during subway construction, leading to varying degrees of subway construction risk [41–44]. According to the report from the Urumqi Municipal Bureau of Geology, the stratigraphic conditions in the study area can be divided into three categories: a soil layer, a soil–rock composite layer, and a rock layer (Figure 3). The geological structure data come from the Urumqi Municipal Bureau of Geology. Most of the subway construction settlement occurs in the first two geological conditions, particularly in the soil area, where the soil is easily compacted by the upper load during subway construction, resulting in surface settlement. Therefore, a spatial correlation exists between surface subsidence and geological conditions in the Urumqi subway construction. As a result, the distribution of stratum conditions is categorized as the first type of risk source for the subway construction environment.

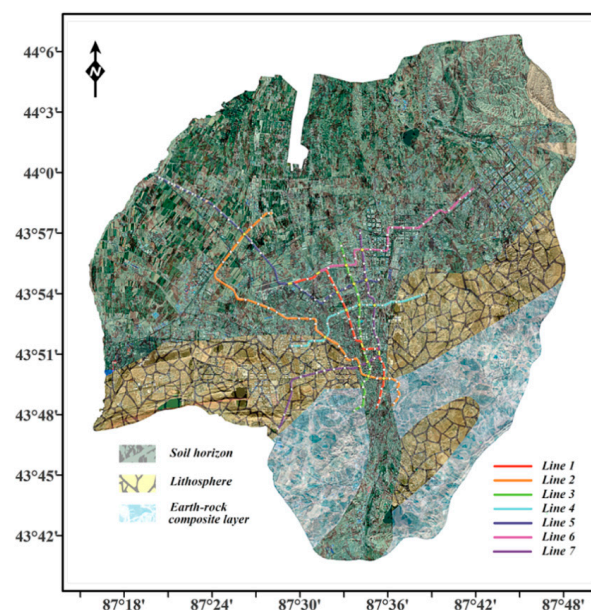


Figure 3. Geological structure of the study area includes the soil layer, rock layer, and soil–rock composite layer.

3.3. Super High-Rise Building Distribution

The construction of subways can disturb the underground soil and disrupt the original stress balance of the soil, which can cause surface subsidence. Additionally, when subway tunnels pass through super high-rise buildings, the impact on the construction of the subway tunnel cannot be generalized with ordinary buildings due to the higher load of super high-rise buildings compared to other buildings [45–48]. According to the “Code for Design of Civil Buildings” GB50352–2005, super high-rise buildings are defined as buildings with more than 40 stories and a height of more than 100 meters [49].

In Urumqi’s Tianshan District, which is the political, economic, cultural, and financial center of the city, there are several subway stations that have been opened, including Line 1 North Gate Station, South Gate Station, Erdaoqiao Station, Xinjiang University Station, and Santunbei Station. According to the “Construction Environment Investigation Report of Urumqi Metro Line 1”, there are 127 super high-rise building sites in this area, making it the most densely populated area of super high-rise buildings in the study area. The dashed boxes b and c in Figure 4a represent the two subsidence areas of Line 1, which are the International Airport Station-Xuanrendun Station, with a maximum displacement of less than 5 mm/year (Figure 4b), and from Erdaoqiao to Nanmen Station, where the maximum displacement exceeds 10 mm/year (Figure 4c). Comparing the settlements of the two areas shows that the distribution of super high-rise buildings is the main factor inducing the deformation of subway construction in this section. Therefore, the distribution of super high-rise buildings is considered the second risk source of the subway construction environment.

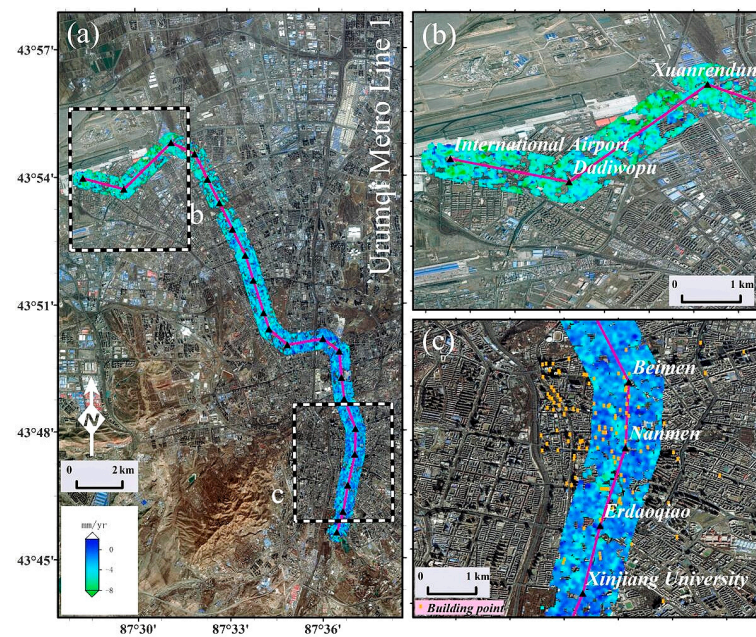


Figure 4. (a) SBAS-InSAR deformation rate map for the 600 m range of Metro Line 1. Regions b and c, marked with white dotted rectangles, are two sinking zones along Line 1, as shown in (b) and (c), respectively.

3.4. Road Network Distribution

The urban road network is a crucial component of urban functionality, and subway lines often overlap with it. However, during subway construction, when the construction of the subway section passes under the existing urban road network, the dynamic load brought by the road network can aggravate the development of land subsidence. According to the report obtained following the analysis of the Urumqi subway line construction settlement method, the larger settlement area of the Urumqi subway line construction is located at the intersection of the urban road network and elevated urban areas. Roads

with different functions (high-speed, national, and ordinary roads) pose different risks to subway construction.

To examine the impact of different road network densities on subway construction, we selected four measurement points with varying road network densities between Balou Station and Wangjialiang Station of Metro Line 1. We conducted a comparative analysis of deformation rates at these points. Figure 5a shows that Point A has no road network nearby, and the road network density of Points B, C, and D increases in the order of $B < C < D$. Figure 5b reveals that the maximum settlement rate is the smallest at Point A, while the deformation rates at Points B, C, and D increase with the road network density. This suggests that there is a positive correlation between surface deformation and road network density during subway construction. Hence, road network distribution is considered a type III risk source for subway construction environments.

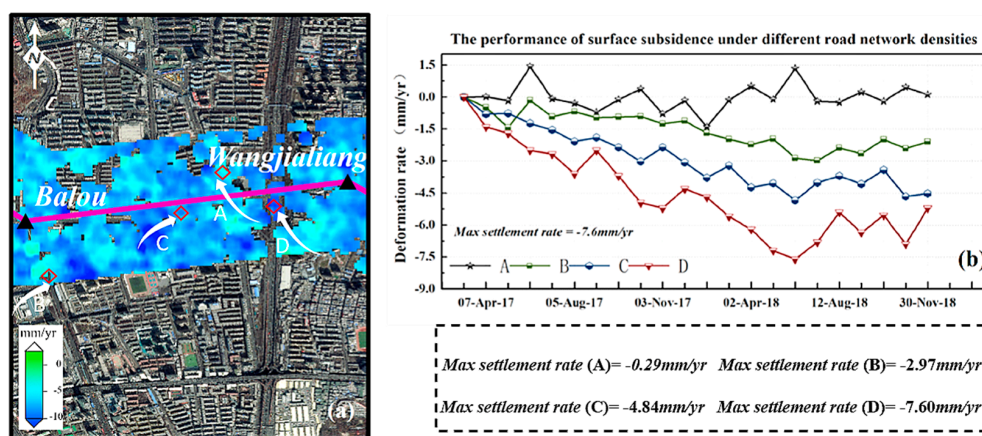


Figure 5. (a) Location of monitoring points under varying road network densities. (b) Shows the settlement rate duration curve for the measuring points under varying road network densities during the monitoring period. The black dotted box below the graph indicates the maximum settlement rate values for Points A, B, C, and D.

3.5. Cluster Building Distribution

Cluster buildings refer to a group of buildings formed by several adjacent buildings in a city that are closely connected in spatial organization. Cluster buildings primarily refer to buildings arranged in a group. The impact of cluster buildings on subway construction is mainly as follows: the additional stress on the base has a deeper influence on depth and a slower attenuation speed, and it causes larger settlements during the subway construction process [50–52]. We quantified the distribution of cluster buildings based on building density and calculated the ratio of the total base area of the building to the occupied area within a certain range [53].

$$Building\ Density = Total\ Base\ Area / Land\ Area \tag{1}$$

To avoid deviations in the results of environmental risk source analysis caused by the combined influence of geological conditions, super high-rise building distribution, and road network distribution, this study used the control variable method and selected four continuous subsidence areas (a, b, c, d in Figure 6e). These four subsidence areas are located in the overlapping area of Beijing Road Main Road and Metro Line 1 in Urumqi. Except for different building densities, there is no significant difference in the subway construction environment and construction methods in the four areas (Table 1). As shown in the green part of Table 1, with the increase in regional building density, the maximum surface displacement during subway construction in the region also increases, and the increasing trend is positively correlated with the building density. Therefore, building density is considered the fourth risk source of subway construction environments.

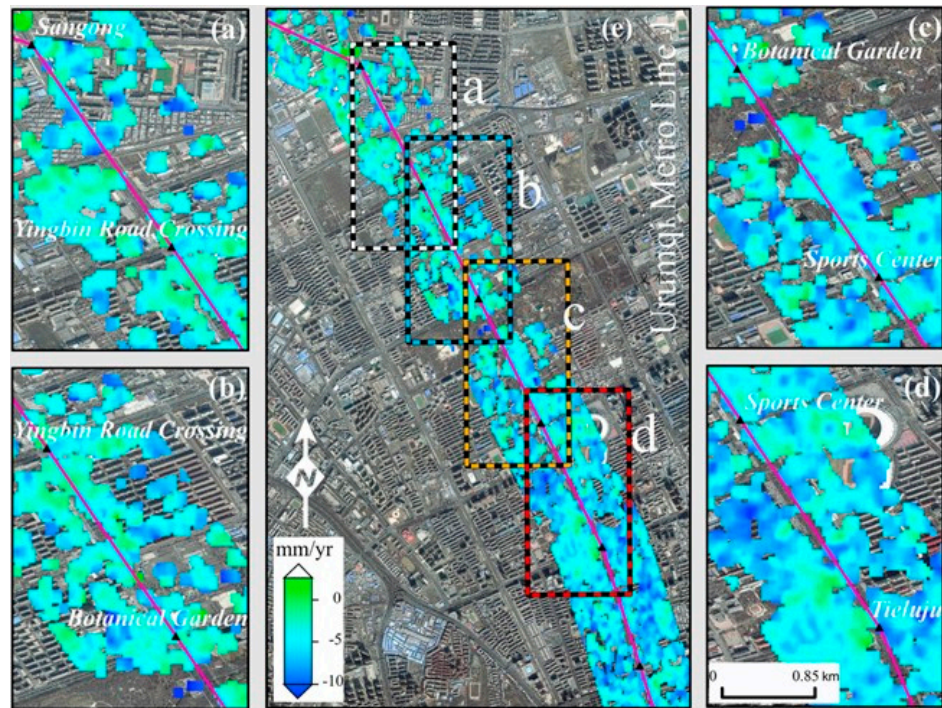


Figure 6. Comparative map for the settlement area of subway construction. (e) SBAS-InSAR deformation rate map for the 600 m range of Sangong Station-Railway Bureau Station of Metro Line 1. The areas a, b, c, and d are marked with dotted rectangles, representing the four control variable areas along Line 1. The enlarged figures are shown as (a), (b), (c), and (d), respectively.

Table 1. a, b, c, and d regional displacement range and environmental variable table. The green padding indicates the area displacement range, and the red triangles present the maximum displacement monitored during area construction.

Area	Data							Environment Variable			
	2	0	-2	-4	-6	-8	-10	-12	Building Density (%)	Super High-Rise Building	Geological Condition
a		1.08		-7.89					23.7	None	soil horizon
b		1.24		-8.38					28.9	None	soil horizon
c		0.87		-11.78					32.6	None	soil horizon
d		-0.52		-12.23					48.2	None	soil horizon

4. Distribution Characteristics of Environmental Risk Sources of Subway Construction in Study Area

Based on the analysis of the environmental risk sources of subway construction in Chapter 2, we obtained the distribution data of the geological conditions in the study area, the POI data of the super high-rise buildings, the distribution data of the road network, and the vector data of the building contours. Using the ArcGIS spatial 3D analysis function, we analyzed the spatial distribution characteristics of the environmental risk sources of subway construction in the study area and classified the risk levels of various risk sources according to the analysis results.

4.1. Spatial Distribution of Geological Conditions

The data on geological conditions in Urumqi were collected from the Urumqi Municipal Bureau of Geology. The distribution of the geological conditions is shown in Figure 3. The geological conditions are divided into three grades based on the distribution of geological conditions in the study area (Table 2).

Table 2. Risk grade and distribution statistics of geological conditions in the study area.

Geological Conditions Risk Level	Geological Condition	Area (km ²)	Proportion (%)
Level I	Soil horizon	1771.3	63
Level II	Earth-rock composite layer	429.1	15.3
Level III	Lithosphere	612.6	21.7

Statistical analysis reveals that the study area is primarily composed of soil layers, which are primarily distributed in the northern part of the study area. A small area is present in the north and south. The rest consists of the soil–rock composite layer. A staggered distribution of the layer of rock is present in the southwest and southeast region of the study area.

4.2. High-Rise Building Distribution

The POI data of super high-rise buildings in the study area were obtained from the Gaode POI spatial data in the first quarter of 2021. Combined with the environmental survey report of Urumqi, the data were preprocessed, and finally, we obtained 350 POI data of super high-rise buildings.

In this study, we utilized the ArcGIS kernel density analysis method to analyze the Point of Interest (POI) data for super high-rise buildings in the study area. The search radius for the kernel density analysis was employed to replace the influence range of the super high-rise buildings on the region. The kernel density analysis value indicates the impact of the super high-rise buildings on the region, with a higher value indicating a greater impact. A distance threshold of 500 meters was set, and the pixel size was set to 200. Based on the kernel density analysis value, we classified the influence range of the super high-rise buildings into four grades (Table 3) and obtained the spatial distribution characteristics of the high-rise buildings in the study area (Figure 7).

Table 3. Statistical table of risk level and influence range of super high-rise buildings in the study area.

High-Rise Building Risk Level	The Influence Range of Nuclear Density	Influence Area (km ²)
Level I	0.00–13.43	2779.28
Level II	13.43–26.87	24.92
Level III	26.87–40.31	6.96
Level IV	40.31–53.75	1.84

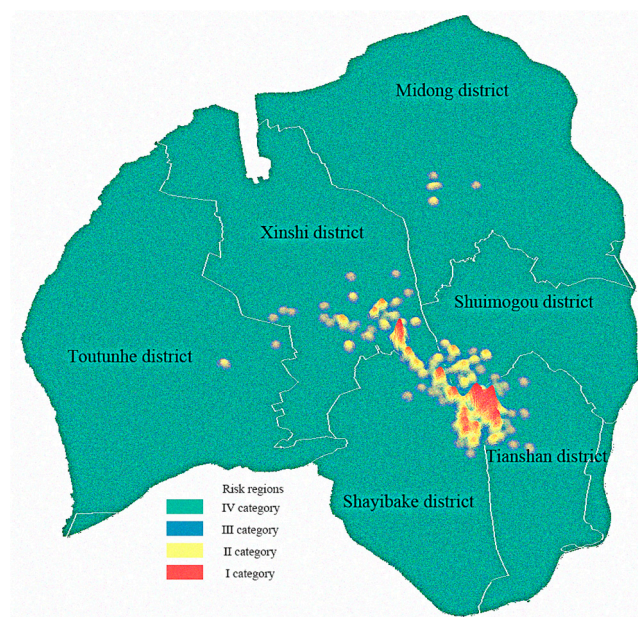


Figure 7. Nuclear density analysis of super high-rise buildings in the study area. The white line in the figure represents the boundary of each regional administrative region.

As shown in Figure 7, the super high-rise buildings in the study area are mainly distributed in the intersection of Tianshan District, Shayibake District, Xinshi District, and Shuimogou District, and they are clustered and distributed, with a trend developing toward the new urban area, which is consistent with the development of Urumqi city center. Finally, the clustering distribution of the super high-rise buildings will significantly impact the risk of subway construction in this area.

4.3. Road Network Distribution

The road network data used in this study were obtained from the “China Natural Disaster Municipal Risk Census Data”. A 500 m * 500 m grid was created within the study area using the ArcGis function to create fishing nets, and the grid was used as a statistical unit to calculate the road length in each grid area to obtain the road network density (Equation (2)).

$$\text{Road Network Density} = \text{Regional Road Network Length} / \text{Grid Area} \quad (2)$$

The road network density is used as a parameter of the road network risk distribution, and the risk level of the road network in the study area was divided into four categories (I, II, III, IV) by using the Jenks natural breakpoint method. The risk level distribution map of road network density in the study area was obtained (Figure 8). The road network in the study area is concentrated in the middle, and the high-density area (dark blue area) is mainly located at the intersection of urban interchanges and main roads. These areas are subjected to large pavement dynamic loads for prolonged periods, which increases the risks associated with subway construction. Table 4 shows the parameters used to evaluate the road network risk level and the proportion of different road network risk levels in the study area.

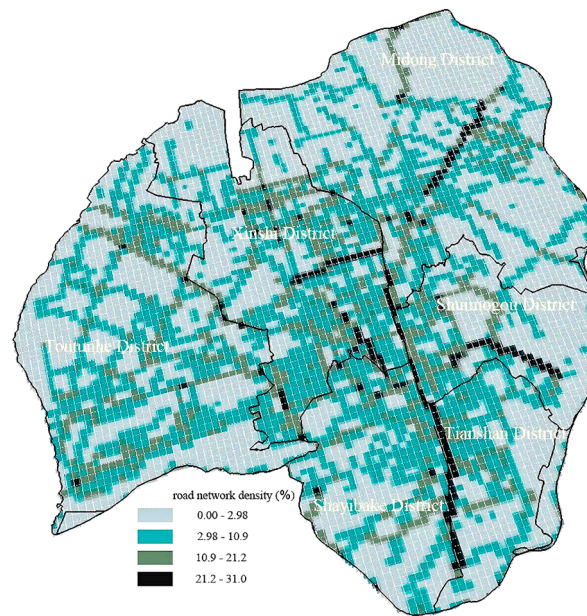


Figure 8. Density risk level and distribution for the road network. White grid for the generated fishing net statistics unit.

Table 4. Risk grade and statistical table for the road network in the study area.

Road Network Density Risk Level	Density Range (%)	Proportion (%)
Level I	0.00–2.98	3.0
Level II	2.98–10.9	7.9
Level III	10.9–21.2	34.6
Level IV	21.2–31.0	54.5

4.4. Cluster Building Division

The building profile data used in this study were obtained from the “China Natural Disaster Housing Risk Census Data.” The formula used for calculating building density (Section 2) was used to establish the fishing net layer and the building contour vector layer (Section 4.3). The building density of each grid was determined by calculating the ratio of the building contour area to the grid area. Based on the building density value of each grid, the risk level was divided into four levels (I, II, III, IV) using the Jenks natural breakpoint method (Table 5). Figure 9 shows the building density distribution map of the study area, where the height of each block represents the building density in that area.

Table 5. Risk level and distribution of cluster buildings.

Building Density Risk Level	Density Range (%)	Proportion (%)
Level I	68.5–100	2.5
Level II	35.4–68.5	14.8
Level III	12.6–35.4	27.6
Level IV	0.00–12.6	55.1

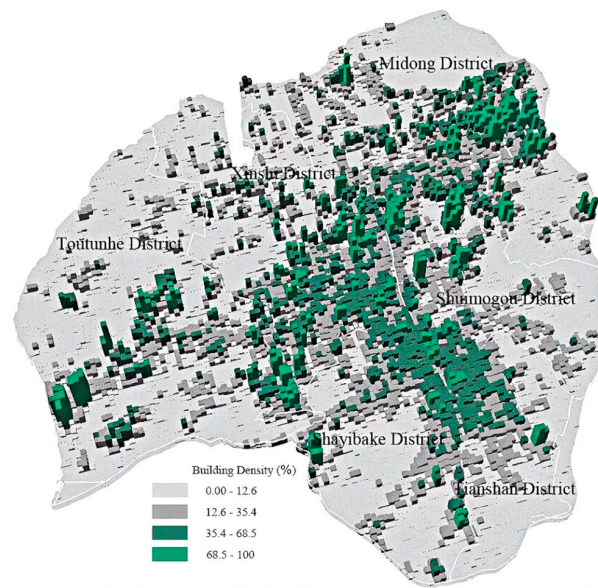


Figure 9. Building density distribution map of the study area.

From the results of the building density analysis shown in Figure 9, we can conclude that the high-density building areas in the study area are primarily located in the northwest of Tianshan District, the northeast of Shayibake District, the central and western part of Toutunhe District, the southeast of Xinshi District, the southeast of Midong District, and the west of Shuimogou District. The risk level and distribution of building density in each region are shown in Table 5.

5. Comprehensive Analysis of the Environmental Risk Faced during the Construction of the Subway in the Study Area

5.1. Introduction of Geometric Partition Theory

Multi-layer raster data overlay analysis (pixel statistics) is often used for mathematical function calculation and the reclassification of raster. It refers to the reclassification of multiple raster data with a unified hierarchy. The available statistical data are mode, maximum, mean, median, minimum, minority, range, standard deviation, sum, and variability. The data analysis principle is shown in Figure 10. The partition operation is based on the classification area of a data set, performs numerical statistical analysis on one or more data sets, and calculates a single output value for each region in the input region data set. The output results can be raster data or tables.

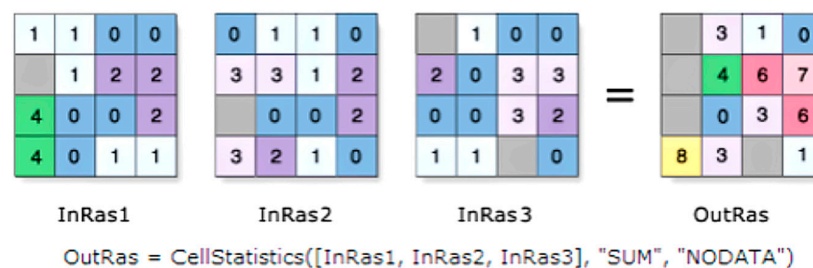


Figure 10. Grid data superposition principle diagram.

5.2. Geometric Partition of the Subway Construction Environmental Risk Sources

In the fourth chapter, we used the partitioning principle in Section 5.1 and the method described in Table 6 to calculate the spatial distribution grid layer for each risk source, a process referred to as geometric partitioning [54]. After partitioning, the study area was divided into 102 zones, and a map of the environmental risk sources for subway

construction was created (Figure 11). The map reveals that the largest partitioned area is 1444, indicating that the environmental risks associated with subway construction in this area include soil layer risk, the risk from grade IV super high-rise buildings, the risk from grade IV road networks, and the risk from grade IV building density. Figure 12 shows the areas of statistical significance greater than 2500 km² and the percentage of the study area.

Table 6. Geometric divisions made on the basis of environmental risk sources associated with the subway construction process in the study area.

Type	Geological Condition	High-Rise Building Risk	Building Density Risk	Road Network Density Risk
Level 1	Soil horizon	I	I	I
Level 2	Rock layer	II	II	II
Level 3	Earth-rock composite layer	III	III	III
Level 4		IV	IV	IV
Partition number	Kilobit	hundred's place	ten's place	units

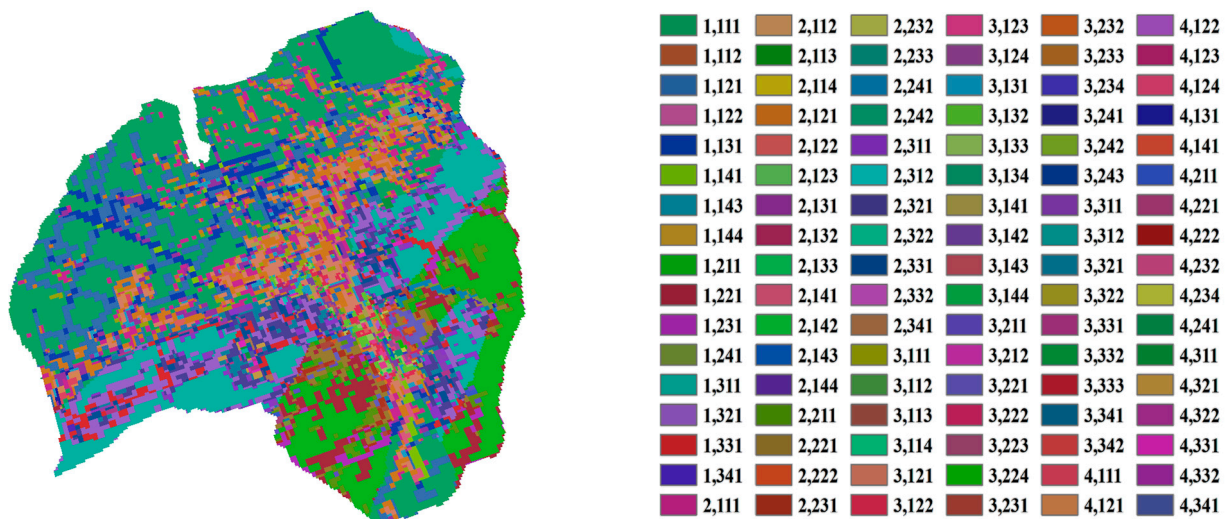


Figure 11. Geometric zoning map of the environmental risk sources associated with the process of subway construction in the study area.

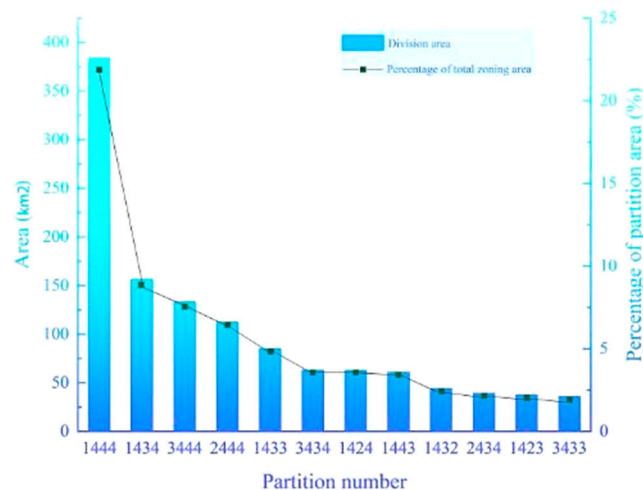


Figure 12. Risk source partition area and percentage of the partition area.

5.3. Environmental Risk Source Zoning Evaluation and Control of Subway Construction

We redefined the risk level of each partition area to accurately depict the comprehensive influence of each risk source on the environmental risk zoning of subway construction in Urumqi. We first obtained the risk assessment value by calculating the weighted average of the risk scores in each partition area. We then defined areas with risk assessment values in the range of [3.75, 2.5), [2.5, 1.75), and [1.75, 1.25) as low-risk, medium-risk, and high-risk areas, respectively. High-risk areas with three or more class I risk sources were defined as level I high-risk areas, medium-risk areas with two or more level I risk sources were defined as level I medium-risk areas, and low-risk areas with one or more level I risk sources were defined as level I low-risk areas. Based on their risk assessment values, the remaining partition areas were defined as II high-risk areas, II medium-risk areas, and II low-risk areas (Figure 13).

Zoning Risk Index, Cumulative 102
(Overall score 1.3–3.8, 3.8 = best environment)

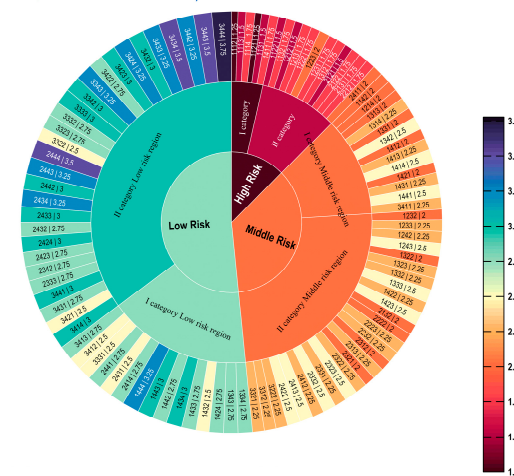


Figure 13. Risk index and classification table for the subway construction risk source zones. The higher the index, the lower the comprehensive risk level of the partition. In other words, the comprehensive impact of the risk source in the region on subway construction is small.

We intersected the planned spatial location of Urumqi Metro Line 1–7 with the geometric partition layer of the subway construction risk source and combined the risk index table to statistically analyze the situation of railway lines crossing the risk area (Table 7). According to Table 8, the comprehensive risk degree of the main crossing risk areas of Metro Line 1–7 is small. However, all lines cross the high-risk zones, the most significant of which is Metro Line 6. There are six high-risk areas.

Table 7. Statistical analysis of the Urumqi Metro Line 1–7 across the subway construction risk source zones.

Metro Lines	Main Crossing Partition	Risk Index	The Highest Level of Risk Zoning	Regional Number	Risk Index
Line 1	1432	2.25	1113	1	1.5
Line 2	3433	3.25	1312	2	1.75
Line 3	2433	3	1122	2	1.5
Line 4	3424	3.25	1312	1	1.75
Line 5	1444	3.25	1232	1	2
Line 6	1433	2.75	1212	5	1.5
Line 7	3444	3.75	1222	3	1.75

Table 8. Risk prevention measures taken for each risk zone.

Zoning Risk Level	Risk Index Interval	Explanation
I category high-risk region	[1.25, 1.75)	Preventive measures must be implemented for various risk sources. The settlement performance of the area must be strictly monitored during construction.
II category high-risk region		Preventive measures must be implemented for each level I risk source.
I category middle-risk region	[1.75, 2.50)	Preventive measures should be identified and implemented for each level I risk source to reduce risk levels
II category middle-risk region		
I category low-risk region	[2.50, 3.75)	The risk is on the edge of tolerance, and it is necessary to pay attention to the possible impact of each level of risk source
II category low-risk region		The risk can be tolerated without taking preventive measures

6. Conclusions

We employed SBAS-InSAR technology to analyze the surface subsidence performance of different areas during the construction of the Urumqi Metro Line 1 and identified the main risk sources of the subway construction environment in Urumqi. We used ArcGIS software to visualize the spatial distribution of each risk source and classify their risk levels. We then carried out a geometric superposition of the spatial distribution layers of each risk source to enable the geometric division of the environmental risk sources of subway construction in the study area. Finally, we redefined the risk index of each partition to draw the following conclusions:

- (1) Four main types of risk sources affect the process of Urumqi subway construction, and these can be classified into natural conditions and human engineering activities. Each risk source control level can be divided into geological conditions (I–III) based on their spatial distribution and spatial density distribution. Additionally, the distribution of super high-rise buildings can be classified into levels I–IV, the road network distribution can be classified into levels I–IV, and the cluster building distribution can be classified into levels I–IV.
- (2) The environmental risk source area of subway construction in the study area is divided into 103 regions, with 12 areas having an area greater than 250,000 km². The largest partition number is 1444, and the partition number with the greatest risk is 1112. The environmental risk source and risk level of subway construction in this area are soil layer, grade I super high-rise building risk, grade I road network risk, and grade II building density risk.
- (3) We graded the comprehensive impact of risk sources on subway construction according to the distribution of risk sources in each sub-region. We also conducted a statistical analysis of Urumqi Metro Line 1–7 crossing the risk source zones and identified the risk control measures needed when the subway line crosses different risk levels.
- (4) In the future planning and construction of the Urumqi subway line, identifying the environmental risk sources of subway construction will assist the planning department in understanding the environmental risk situation surrounding the subway planning line. This information will provide a foundation for the rational planning and adjustment of regional subway lines. The subway construction company will be able to determine the environmental risk level of the subway’s construction and take necessary risk control measures in advance based on the intersection of the actual subway line location and the environmental risk source zoning layer. This will help to mitigate the risk of inconsistency between the judgment results of engineering design drawings and engineering practice due to insufficient consideration of risk factors during the planning and design stage.

Author Contributions: Conceptualization, Y.Y. and Y.Q.; methodology, Y.Y. and L.X.; software, Y.Y. and Y.Z.; validation, Y.Y. and X.M.; formal analysis, Y.Y. and Z.G.; investigation, Y.Y. and Y.Z.; resources, Y.Q. and L.X.; data curation, Y.Y. and Y.Z.; writing—original draft preparation, Y.Y.; writing—review and editing, Y.Y. and Y.Z.; visualization, Y.Q. and Y.Z.; supervision, Y.Q.; project administration, Y.Q.; funding acquisition, Y.Q. All authors have read and agreed to the published version of the manuscript.

Funding: This study was financially supported by the Natural Science Foundation of Xinjiang Province (Grant No. 2021D01C073).

Institutional Review Board Statement: Not applicable.

Informed Consent Statement: Not applicable.

Data Availability Statement: All data generated and analyzed during this study are included in this article.

Conflicts of Interest: The authors declare no conflict of interest.

References

- Mohammadi, S.D.; Naseri, F.; Alipoor, S. Development of Artificial Neural Networks and Multiple Regression Models for the NATM Tunnelling-Induced Settlement in Niayesh Subway Tunnel, Tehran. *Bull. Eng. Geol. Environ.* **2015**, *74*, 827–843. [[CrossRef](#)]
- Cui, Z.-D.; Tan, J. Analysis of Long-Term Settlements of Shanghai Subway Line 1 Based on the in Situ Monitoring Data. *Nat. Hazards* **2015**, *75*, 465–472. [[CrossRef](#)]
- Zhang, Q.; Wang, J.; Zhang, H. Attribute Recognition Model and Its Application of Risk Assessment for Slope Stability at Tunnel Portal. *J. Vibroeng.* **2017**, *19*, 2726–2738. [[CrossRef](#)]
- Yu, J.; Zhong, D.; Ren, B.; Tong, D.; Hong, K. Probabilistic Risk Analysis of Diversion Tunnel Construction Simulation. *Comput.-Aided Civ. Infrastruct. Eng.* **2017**, *32*, 748–771. [[CrossRef](#)]
- Zhou, Z.; Li, Q.; Wu, W. Developing a Versatile Subway Construction Incident Database for Safety Management. *J. Constr. Eng. Manag.-Asce* **2012**, *138*, 1169–1180. [[CrossRef](#)]
- Liu, J.; Du, Z.; Ma, L.; Liu, C. Identification and Assessment of Subway Construction Risk: An Integration of AHP and Experts Grading Method. *Adv. Civ. Eng.* **2021**, *2021*, 6661099. [[CrossRef](#)]
- Fu, L.; Wang, X.; Zhao, H.; Li, M. Interactions among Safety Risks in Metro Deep Foundation Pit Projects: An Association Rule Mining-Based Modeling Framework. *Reliab. Eng. Syst. Saf.* **2022**, *221*, 108381. [[CrossRef](#)]
- Sun, C. *Research on Safety Risk Control Technology and Its Application in Beijing Metro Approaching Construction*; Beijing Jiaotong University: Beijing, China, 2014. (In Chinese)
- Stirbys, A.F.; Radwanski, Z.R.; Proctor, R.J.; Escandon, R.F. Los Angeles Metro Rail Project—Geologic and Geotechnical Design and Construction Constraints. *Eng. Geol.* **1999**, *51*, 203–224. [[CrossRef](#)]
- Li, S. *Study on Risk Management of Subway Construction to Surroundings Environment*; Xi'an University Architecture and Technology: Xi'an, China, 2011. (In Chinese)
- Han, M.; Li, Z.; Mei, G.; Bao, X.; Jia, J.; Liu, L.; Li, Y. Characteristics of Subway Excavation in Soft Soil and Protective Effects of Partition Wall on the Historical Building and Pile Foundation Building. *Bull. Eng. Geol. Environ.* **2022**, *81*, 307. [[CrossRef](#)]
- Xiao, Y. *Study on the Impact of High-Rise Building on the Safety of Subway Station*; Chongqing Jiaotong University: Chongqing, China, 2017. (In Chinese)
- Shen, Z. *Impact of the Super High-Rise Building Constructing and Using Stage on Closely Adjacent Operating Metro Tunnels*; Beijing Jiaotong University: Beijing, China, 2017. (In Chinese)
- Xue, Y.; Li, X.; Li, G.; Qiu, D.; Gong, H.; Kong, F. An Analytical Model for Assessing Soft Rock Tunnel Collapse Risk and Its Engineering Application. *Geomech. Eng.* **2020**, *23*, 441–454. [[CrossRef](#)]
- Xu, Z.; Cai, N.; Li, X.; Xian, M.; Dong, T. Risk Assessment of Loess Tunnel Collapse during Construction Based on an Attribute Recognition Model. *Bull. Eng. Geol. Environ.* **2021**, *80*, 6205–6220. [[CrossRef](#)]
- Meng, G.; Ye, Y.; Wu, B.; Luo, G.; Zhang, X.; Zhou, Z.; Sun, W. Risk Assessment of Shield Tunnel Construction in Karst Strata Based on Fuzzy Analytic Hierarchy Process and Cloud Model. *Shock Vib.* **2021**, *2021*, 7237136. [[CrossRef](#)]
- Zhou, Y.; Liu, Y.; Chen, Q.; Ou, X.; Li, Y. Case Study of an Underpinning Pile Foundation for an Interval Tunnel Crossing an Existing Bridge. *Appl. Sci.* **2022**, *12*, 12566. [[CrossRef](#)]
- Li, C.; Zhang, W.; Wang, X.; Pan, B.; Zhu, H.; Spencer, B.F. Modeling Dynamic Responses of a Cross-River Road Shield Tunnel under Stochastic Vehicle Loads. *Tunn. Undergr. Space Technol.* **2020**, *102*, 103432. [[CrossRef](#)]
- Jun, S.; Jun, L.; Yong, W. Analysis of the influence of subway entrance excavation on tunnel and adjacent buildings. *IOP Conf. Series. Earth Environ. Sci.* **2019**, *371*, 022037.
- Xu, Z.; Li, X. Analysis of Settlement Caused by Tunnel Underneath Existing Railway after Construction. *Adv. Mater. Res.* **2013**, *2592*, 534. [[CrossRef](#)]

21. Luo, C.; Cheng, Y.; Bai, Z.; Shen, T.; Wu, X.-Y.; Wang, Q. Study on Settlement and Deformation of Urban Viaduct Caused by Subway Station Construction under Complicated Conditions. *Adv. Civ. Eng.* **2021**, *2021*, 6625429. [[CrossRef](#)]
22. Ren, D.-J.; Shen, S.-L.; Cheng, W.-C.; Zhang, N.; Wang, Z.-F. Geological Formation and Geo-Hazards during Subway Construction in Guangzhou. *Environ. Earth Sci.* **2016**, *75*, 934. [[CrossRef](#)]
23. Jin, D.; Yuan, D.; Li, X.; Zheng, H. Analysis of the Settlement of an Existing Tunnel Induced by Shield Tunneling Underneath. *Tunn. Undergr. Space Technol.* **2018**, *81*, 209–220. [[CrossRef](#)]
24. Gan, X.; Yu, J.; Gong, X.; Zhu, M. Characteristics and Countermeasures of Tunnel Heave Due to Large-Diameter Shield Tunneling Underneath. *J. Perform. Constr. Facil.* **2020**, *34*, 04019081. [[CrossRef](#)]
25. Ng, C.W.W.; Boonyarak, T.; Masin, D. Effects of Pillar Depth and Shielding on the Interaction of Crossing Multitunnels. *J. Geotech. Geoenviron. Eng.* **2015**, *141*, 04015021. [[CrossRef](#)]
26. Lai, H.; Zheng, H.; Chen, R.; Kang, Z.; Liu, Y. Settlement Behaviors of Existing Tunnel Caused by Obliquely Under-Crossing Shield Tunneling in Close Proximity with Small Intersection Angle. *Tunn. Undergr. Space Technol.* **2020**, *97*, 103258. [[CrossRef](#)]
27. Merlini, D.; Stocker, D.; Falanesca, M.; Schuerch, R. The Ceneri Base Tunnel: Construction Experience with the Southern Portion of the Flat Railway Line Crossing the Swiss Alps. *Engineering* **2018**, *4*, 235–248. [[CrossRef](#)]
28. Lian, X.; Wu, Y.; Ge, L.; Du, Z.; Liu, X. DInSAR Monitoring of Surface Subsidence by Fusing Sentinel-1A and-1B Data to Improve Time Resolution in a Mining Area. *Can. J. Remote Sens.* **2021**, *47*, 596–606. [[CrossRef](#)]
29. Xie, Z.; Chen, G.; Meng, X.; Zhang, Y.; Qiao, L.; Tan, L. A Comparative Study of Landslide Susceptibility Mapping Using Weight of Evidence, Logistic Regression and Support Vector Machine and Evaluated by SBAS-InSAR Monitoring: Zhouqu to Wudu Segment in Bailong River Basin, China. *Environ. Earth Sci.* **2017**, *76*, 313. [[CrossRef](#)]
30. Li, Y.; Yang, K.; Zhang, J.; Hou, Z.; Wang, S.; Ding, X. Research on Time Series InSAR Monitoring Method for Multiple Types of Surface Deformation in Mining Area. *Nat. Hazards* **2022**, *114*, 2479–2508. [[CrossRef](#)]
31. Du, Y.; Feng, G.; Peng, X.; Li, Z. Subsidence Evolution of the Leizhou Peninsula, China, Based on InSAR Observation from 1992 to 2010. *Appl. Sci.* **2017**, *7*, 466. [[CrossRef](#)]
32. Tao, Q.; Wang, F.; Guo, Z.; Hu, L.; Yang, C.; Liu, T. Accuracy Verification and Evaluation of Small Baseline Subset (SBAS) Interferometric Synthetic Aperture Radar (InSAR) for Monitoring Mining Subsidence. *Eur. J. Remote Sens.* **2021**, *54*, 641–662. [[CrossRef](#)]
33. Wang, H.; Feng, G.; Xu, B.; Yu, Y.; Li, Z.; Du, Y.; Zhu, J. Deriving Spatio-Temporal Development of Ground Subsidence Due to Subway Construction and Operation in Delta Regions with PS-InSAR Data: A Case Study in Guangzhou, China. *Remote Sens.* **2017**, *9*, 1004. [[CrossRef](#)]
34. Zhao, Y.; Zhou, L.; Wang, C.; Li, J.; Qin, J.; Sheng, H.; Huang, L.; Li, X. Analysis of the Spatial and Temporal Evolution of Land Subsidence in Wuhan, China from 2017 to 2021. *Remote Sens.* **2022**, *14*, 3142. [[CrossRef](#)]
35. Zhang, Y.; Liu, Y.; Jin, M.; Jing, Y.; Liu, Y.; Liu, Y.; Sun, W.; Wei, J.; Chen, Y. Monitoring Land Subsidence in Wuhan City (China) Using the SBAS-InSAR Method with Radarsat-2 Imagery Data. *Sensors* **2019**, *19*, 743. [[CrossRef](#)]
36. Shi, W.; Chen, G.; Meng, X.; Jiang, W.; Chong, Y.; Zhang, Y.; Dong, Y.; Zhang, M. Spatial-Temporal Evolution of Land Subsidence and Rebound over Xi'an in Western China Revealed by SBAS-InSAR Analysis. *Remote Sens.* **2020**, *12*, 3756. [[CrossRef](#)]
37. Xiao, B.; Zhao, J.; Li, D.; Zhao, Z.; Xi, W.; Zhou, D. The Monitoring and Analysis of Land Subsidence in Kunming (China) Supported by Time Series InSAR. *Sustainability* **2022**, *14*, 12387. [[CrossRef](#)]
38. Hu, B.; Yang, B.; Zhang, X.; Chen, X.; Wu, Y. Time-Series Displacement of Land Subsidence in Fuzhou Downtown, Monitored by SBAS-InSAR Technique. *J. Sens.* **2019**, *2019*, 3162652. [[CrossRef](#)]
39. Hussain, M.A.; Chen, Z.; Shoaib, M.; Shah, S.U.; Khan, J.; Ying, Z. Sentinel-1A for Monitoring Land Subsidence of Coastal City of Pakistan Using Persistent Scatterers In-SAR Technique. *Sci. Rep.* **2022**, *12*, 5294. [[CrossRef](#)]
40. Hu, B.; Chen, B.; Na, J.; Yao, J.; Zhang, Z.; Du, X. Urban Surface Deformation Management: Assessing Dangerous Subsidence Areas through Regional Surface Deformation, Natural Factors, and Human Activities. *Sustainability* **2022**, *14*, 10487. [[CrossRef](#)]
41. Li, Y.; Jin, X.; Feng, Y.; Luo, W. Effect of Soft Layer on Seismic Response of Subway Station in Layered Stratum. *J. Vibroeng.* **2016**, *18*, 1602–1616. [[CrossRef](#)]
42. Luo, J.; Miao, L. Research on Dynamic Creep Strain and Settlement Prediction under the Subway Vibration Loading. *SpringerPlus* **2016**, *5*, 1252. [[CrossRef](#)]
43. Jiang, X.; Hou, L.; Shang, S.; Xu, L.; Yu, H. Physical Modeling of a Shallow-Buried Metro Tunnel in the Soft Loess Layer Using Similarity Theory. *Adv. Civ. Eng.* **2022**, *2022*, 5587116. [[CrossRef](#)]
44. Feng, X.; Hou, D.; Huang, Z. The Influence of Shield Tunneling Characteristics on the Safety of Buildings Above-Case Study for Shanghai Zone. *Sustainability* **2022**, *14*, 13391. [[CrossRef](#)]
45. Liu, J.; Qi, T.; Wu, Z. Analysis of Ground Movement Due to Metro Station Driven with Enlarging Shield Tunnels under Building and Its Parameter Sensitivity Analysis. *Tunn. Undergr. Space Technol.* **2012**, *28*, 287–296. [[CrossRef](#)]
46. Li, M.; Zhang, X.; Bai, Z.; Xie, H.; Chen, B. Land Subsidence in Qingdao, China, from 2017 to 2020 Based on PS-InSAR. *Int. J. Environ. Res. Public Health* **2022**, *19*, 4913. [[CrossRef](#)] [[PubMed](#)]
47. Yu-Geng, T.; Tung-Chin, K.G. Probability Based Analysis of Excavation-Induced Damage Potential of Buildings Using a Simplified Evaluation Model. *Disaster Adv.* **2012**, *5*, 332–340.
48. Yuan, C.; Liu, Y.; Li, C.; Wang, C. Analysis of Settlement Characteristics of an Ultrahigh-Rise Building in the Construction Process. *Sci. Surv. Mapp.* **2017**, *42*, 172–177.

49. Ministry of Construction of the People's Republic of China. *Code for Design of Civil Buildings-GB50352-2005*; Ministry of Construction of the People's Republic of China: Beijing, China, 2005. (In Chinese)
50. Usui, H.; Asami, Y. Size Distribution of Building Lots and Density of Buildings and Road Networks: Theoretical Derivation Based on Gibrat's Law and Empirical Study of Downtown Districts in Tokyo. *Int. Reg. Sci. Rev.* **2020**, *43*, 229–253. [[CrossRef](#)]
51. Song, Y.; Chen, X.; Zou, B.; Mu, J.; Hu, R.; Cheng, S.; Zhao, S. Monitoring Study of Long-Term Land Subsidence during Subway Operation in High-Density Urban Areas Based on DInSAR-GPS-GIS Technology and Numerical Simulation. *Cmes-Comput. Model. Eng. Sci.* **2023**, *134*, 1021–1039. [[CrossRef](#)]
52. Zhao, Y.; Liu, C. The Role of Load of Clustered Architecture on Land Subsidence. *Hydrogeol. Eng. Geol.* **2016**, *43*, 162–170. (In Chinese)
53. Li, L.; Zheng, X.; Xiang, W. A Study on Site Coverage Spatial Distribution Pattern of Beijing City Based on Gis. *China Popul. Environ.* **2008**, *18*, 122–127. (In Chinese)
54. Xie, L. Reverse Slope' Toppling Deformation Characteristics Based on Geological Geometric Partitioning. *Sci. Technol. Eng.* **2018**, *18*, 32–37. (In Chinese)

Disclaimer/Publisher's Note: The statements, opinions and data contained in all publications are solely those of the individual author(s) and contributor(s) and not of MDPI and/or the editor(s). MDPI and/or the editor(s) disclaim responsibility for any injury to people or property resulting from any ideas, methods, instructions or products referred to in the content.